

Microstructures and mechanical behavior of Inconel 718 fabricated by selective laser melting

K.N. Amato^{a,b,*}, S.M. Gaytan^{a,b}, L.E. Murr^{a,b}, E. Martinez^{a,b}, P.W. Shindo^{a,b},
J. Hernandez^{a,b}, S. Collins^c, F. Medina^b

^a Department of Metallurgical and Materials Engineering, The University of Texas at El Paso, El Paso, TX 79968, USA

^b W.M. Keck Center for 3D Innovation, The University of Texas at El Paso, El Paso, TX 79968, USA

^c Directed MFG, 1007 South Heatherwild Boulevard, Suite 700, Pflugerville, TX 78660, USA

Received 17 August 2011; received in revised form 28 October 2011; accepted 19 December 2011

Available online 1 March 2012

Abstract

In this study Inconel 718 cylinders were fabricated by selective laser melting in either argon or nitrogen gas from a pre-alloyed powder. As-fabricated cylinders oriented in the build direction (z -axis) and perpendicular to the build direction (x -axis) exhibited columnar grains and arrays of γ'' (body-centered tetragonal) Ni_3Nb oblate ellipsoidal precipitates oriented in a strong [200] texture determined by combined optical metallography, transmission electron microscopy, and X-ray diffraction analysis. Fabricated and hot isostatic pressed (HIP) components exhibited a more pronounced [200] columnar γ'' phase precipitate architecture parallel to the laser beam or build direction (spaced at $\sim 0.8 \mu\text{m}$), and a partially recrystallized fcc grain structure. Fabricated and annealed (1160 °C for 4 h) components were $\sim 50\%$ recrystallized and the recrystallized regions contained spheroidal γ' precipitates distributed in a dense field of fine γ'' precipitates. The γ'' precipitates were always observed to be coincident with {100} planes of the γ -fcc NiCr matrix. Some δ phase precipitates in the unrecrystallized/recrystallized interfaces and recrystallized grain boundaries were also observed in the annealed samples. The microindentation (Vickers) hardness was 3.9 GPa for the as-fabricated materials, 5.7 GPa for the HIP material, and 4.6 GPa for the annealed material. Corresponding tensile properties were comparable with wrought Inconel 718 alloy.

Published by Elsevier Ltd. on behalf of Acta Materialia Inc.

Keywords: Nickel alloys; Solidification; Microstructure; Precipitation; Texture

1. Introduction

Nickel-based superalloys with a broad range of alloy compositions have found a wide range of industrial and aerospace applications over the past four decades in cast, wrought and powder metallurgy forms, especially after the development of pre-alloyed powders by rapid solidification technologies [1,2]. Inconel 718, a Ni–Fe–Cr (or Ni–Cr solid solution hardened) austenite (γ) has found particular applications in gas turbine blades, combustors,

turbocharger rotors, a variety of corrosion containments and structural applications up to ~ 700 °C. In its wrought form Inconel 718 normally exhibits three intermetallic precipitation phases: γ' , having the composition $\text{Ni}_3(\text{Al}, \text{Ti}, \text{Nb})$ and a cubic (ordered face-centered) Ll_2 crystal structure; γ'' , having the composition Ni_3Nb and a body-centered tetragonal (bct) (DO_{22}) crystal structure; an orthorhombic (DO_a) δ phase having the composition Ni_3Nb . The nominal base composition is 51Ni–22Fe–19Cr–5Nb–3Mo–1Co (plus small additions of Ti ($\sim 1\%$) and Al ($\sim 0.5\%$)). Studying alloys with a base composition Ni–25Fe–16Cr, Kirman and Warrington [3] showed that both the γ' and γ'' phases occur when 1.8Ti and 3.5Nb were added, but when the Ti content was increased to 3.5Ti only the γ' phase was obtained, while increasing the Nb content to 6Nb allowed

* Corresponding author at: Department of Metallurgical and Materials Engineering, The University of Texas at El Paso, El Paso, TX 79968, USA. Tel.: +1 915 256 9952; fax: +1 915 747 8036.

E-mail address: knamato@miners.utep.edu (K.N. Amato).

only the γ'' phase to form. The γ' precipitates are cuboidal or spherical, while the γ'' precipitates are lenticular, disc-shaped (oblate spheroid) particles with the following orientation relationships [4,5]:

$$(001)\gamma'' \parallel \{001\}\gamma; [100]\gamma'' \parallel \langle 100 \rangle \gamma$$

In a recent study of Inconel 718 produced by electron beam melting (EBM) an additive (layer) manufacturing process utilizing pre-alloyed, atomized powder Strondl et al. [6] observed columnar, [200] textured γ grains having low angle boundaries containing coarse (50–100 nm) γ'' precipitates. Coarse (<2 μm) (Ti, Nb)(C, N, B) type precipitates with a B1 structure were also observed to be aligned along the growth (or layer building) direction. The $(001)\gamma \parallel (001)\gamma''$ orientation relationship was also confirmed.

In the present study pre-alloyed, rapidly solidified (atomized) Inconel 718 powder served as a precursor for the production of additive manufactured components using selective laser melting (SLM). In contrast to EBM, a vacuum environment process, the SLM process utilizes an inert atmosphere (argon or nitrogen gas). Consequently, different process parameters produce cooling variations which can affect the residual microstructure and mechanical behavior [7]. This study represents a comprehensive microstructural and mechanical behavior characterization using optical metallography (OM), scanning electron microscopy (SEM) and transmission electron microscopy (TEM) employing energy-dispersive X-ray spectrometry (EDS), and X-ray diffraction (XRD) analysis. The mechanical properties (hardness and tensile strength, including fracture surface analysis by SEM) were also measured for as-fabricated and heat-treated components.

2. Experimental methods

The precursor, pre-alloyed atomized Inconel 718 powder, had the composition 53.5Ni–19Cr–18.3Fe–5Nb–3Mo–1Ti–0.43Al. Fig. 1a shows an SEM view illustrating the powder size and morphology, with an average particle size of 17 μm . An OM view of a mounted, polished and etched particle section of the microdendritic structure is shown in Fig. 1b.

Fig. 2 shows a schematic view representing the EOS M270 SLM system which utilized a 200 W Yb:YAG fiber laser (Fig. 2-1). Cylindrical components measuring 1.6 cm diameter \times 8.75 cm length were fabricated in both a vertical and horizontal build orientation, with the cylinder axis parallel to or perpendicular to the beam direction, respectively. The 100 μm diameter laser beam was scanned at 800 or 1200 mm s^{-1} in either argon or nitrogen gas environments surrounding the building components. The build platform (Fig. 2-5) was preheated to 80 $^{\circ}\text{C}$ and maintained at that temperature. Re-coater formed and melted layers (Fig. 2-6) were alternately scanned along the x - or y -axis (at 90 $^{\circ}$). The as-fabricated cylindrical specimens were

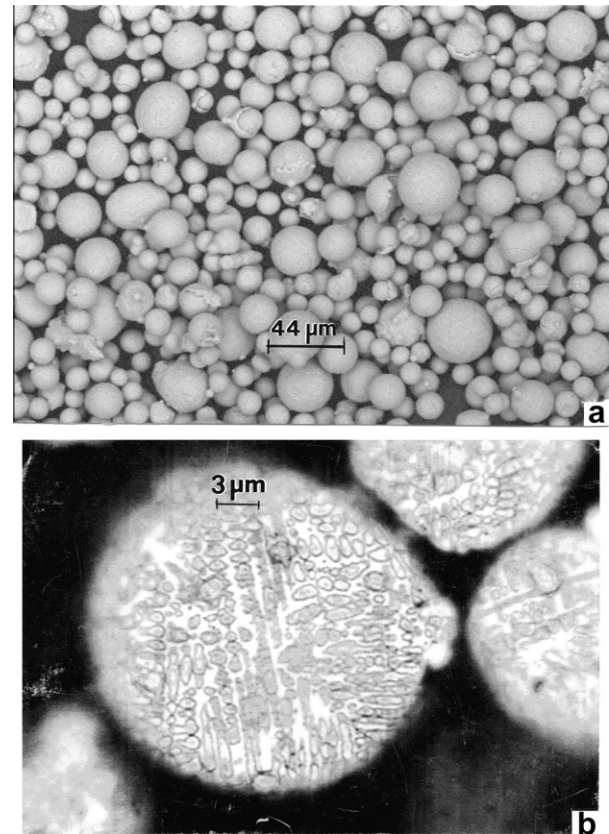


Fig. 1. The pre-alloyed (Inconel 718) precursor powder. (a) Low magnification SEM image showing the range of powder sizes and spherical morphology. (b) Optical metallographic image of a powder particle etched cross-section showing the internal microdendritic microstructure.

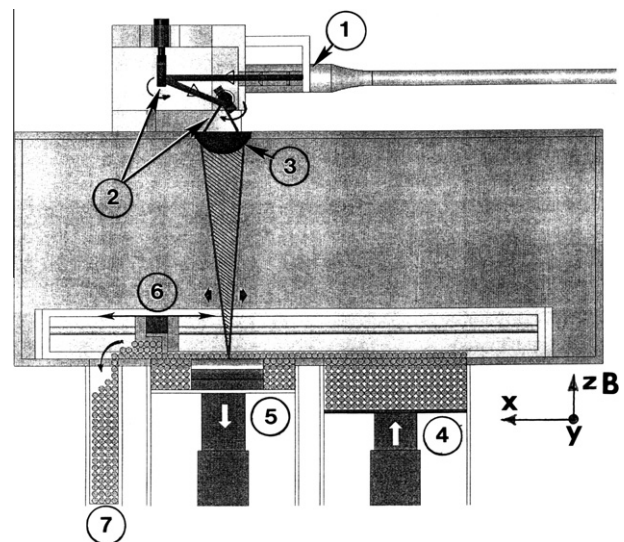


Fig. 2. Components indicated are: (1) laser input; (2) mirror system; (3) beam focus lens; (4) powder feed system; (5) build platform; (6) re-coater system for powder layer formation; (7) powder recovery/recycle bin.

annealed at 982 $^{\circ}\text{C}$ for 0.5 h under vacuum and then hot isostatic pressed (HIP) at 1163 $^{\circ}\text{C}$ at 0.1 GPa pressure for

4 h in argon. As-fabricated samples were also annealed in argon at 1160 °C for 4 h for comparison.

The microstructures for both the as-fabricated and HIP/annealed samples were observed by OM initially utilizing a Reichert MEF-4 A/M metallograph using digital imaging. Coupons were cut as horizontal (transverse) reference plane samples perpendicular to the beam direction (or build direction) or as vertical (longitudinal) reference plane samples parallel to the build direction. These coupons were mounted, ground, polished, and electro-etched in a solution of 70 ml of phosphoric acid and 30 ml of water at room temperature, using 5 V for etching times of between 5 and 120 s.

XRD spectra of the powder as well as extracted coupons from the transverse (horizontal) and longitudinal (vertical) reference planes from the fabricated cylinders are shown in Fig. 1. The XRD system was a Bruker AXS-D8 Discover machine using a Cu target.

SEM imaging (as in Fig. 1a) employed a Hitachi S-4800 field emission SEM, fitted with an EDAX energy-dispersive X-ray spectrometry (EDS) system for chemical analysis and elemental mapping, and normally operated at 20 kV in the secondary electron or backscatter electron emission imaging modes. Extracted coupons were also examined by TEM using a Hitachi H-9500 high resolution digital imaging system, operated at 300 kV. Specimens for TEM were prepared by grinding extracted coupons to a thickness of $\sim 200 \mu\text{m}$, punching 3 mm discs, mechanically dimpling the discs, and electropolishing them in a Tenu-pol-5 dual jet system at a temperature of $\sim -30 \text{ }^\circ\text{C}$, using an etchant consisting of 200 ml of perchloric acid and 800 ml of methanol, at 13 V. The TEM was also fitted with a goniometer tilt stage which facilitated contrast control, selected area electron diffraction (SAED) pattern manipulation, and dark field imaging. The TEM was also fitted with an EDAX energy-dispersive X-ray spectrometer with a spatial resolution of chemical elements of roughly 20 nm on a side.

Microindentation (Vickers HV) hardness and macroindentation hardness (Rockwell C-scale HRC) using loads of 0.25 and 1.5 N, respectively, were made on specimen sections extracted from z -axis and x -axis cylinders parallel or perpendicular to the build direction and representing the horizontal and vertical reference planes correspondingly perpendicular to or parallel to the build direction. The microindentation hardness tester was a Shimadzu HMV-2000 digital measuring system. Measurements were averages for 20 HV values and 10 HRC values.

Tensile specimens were machined from the as-fabricated cylinders built in Ar and N_2 gas and HIP/annealed cylinders representing both the vertical (z -axis) built specimens as well as the horizontal (x -axis) built specimens. Tensile testing was performed in a Universal Testing machine at room temperature ($\sim 300 \text{ K}$) at a strain rate of $\sim 10^{-3} \text{ s}^{-1}$. Fracture surface examination was also performed by SEM.

3. Results and discussion

3.1. Microstructures of SLM fabricated and treated components

Fig. 3a shows the appearance of melt pools and layer development as a result of alternating (x - y) melt scans every other layer when viewed in the vertical reference plane (in the build direction) for an x -axis oriented cylinder. This melt pool layer appearance has been observed after the SLM fabrication of Ti-6Al-4V components using a similar scanning strategy by Thijs et al. [7]. The melt pool width is observed to vary from ~ 75 to $100 \mu\text{m}$, while the average layer thickness is observed to be $\sim 50 \mu\text{m}$. The magnified view in Fig. 3b also shows the development of columnar grains and other regular columnar microstructures essentially parallel to the build direction (indicated by the arrow). When viewed in a three-dimensional (3-D) section, as shown in Fig. 4, the irregular columnar microstructures shown in Fig. 3b in the vertical reference plane are observed to compose an equiaxed or regular spatial columnar architecture having dimensions between 0.5 and

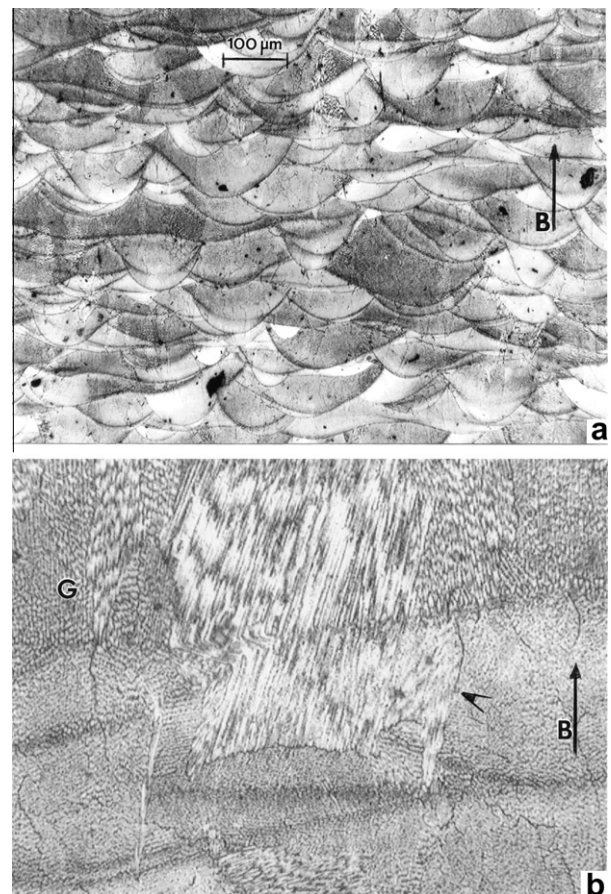


Fig. 3. (a) Melt pool overlap and layer development observed in the vertical reference plane (parallel to the build direction shown by the arrow) for an x -axis oriented, as-fabricated cylinder (in argon). (b) Magnified view showing columnar grain structure (G) and fine columnar special features (shown by arrow). B, build direction.

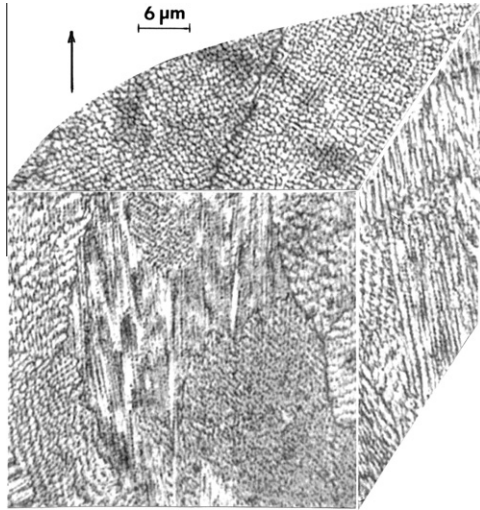


Fig. 4. 3-D optical metallograph (OM image) composite showing the details of columnar grains and fine arrays relative to the build direction shown by the arrow (top left) for an as-fabricated (x -axis) cylinder in argon gas.

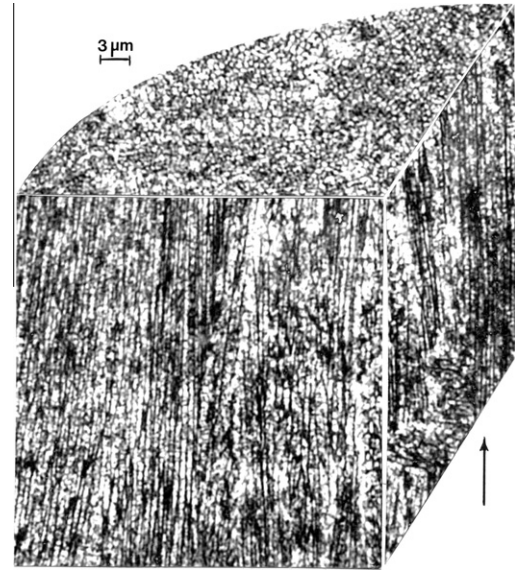


Fig. 6. 3-D OM composite view for a cylindrical component (z -axis) fabricated in argon and HIP in argon. The build direction is indicated by the arrow (bottom right).

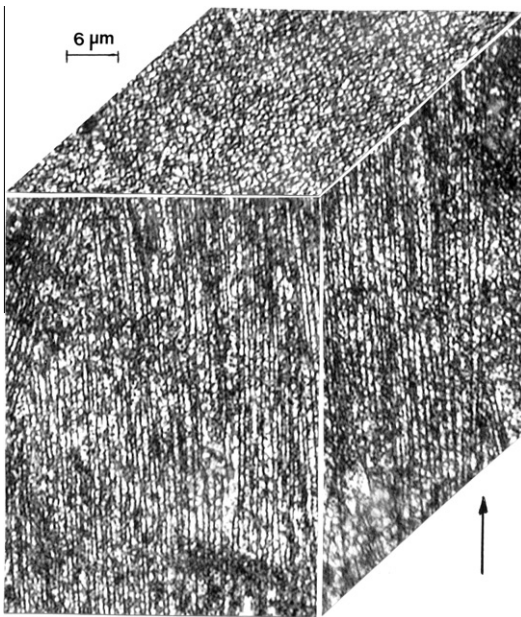


Fig. 5. 3-D OM composite view for a cylindrical component (x -axis) fabricated in argon and HIP in argon. The build direction is indicated by the arrow (bottom right).

1 μm , as observed in the horizontal reference plane section showing these arrays.

While Fig. 4 shows these columnar architecture arrays for an x -axis cylinder built in an argon gas environment, Fig. 5 shows a more regular columnar architecture spatially identical to Fig. 4 for an x -axis oriented cylinder built in argon gas and HIP at 1163 $^{\circ}\text{C}$ for 4 h at 0.1 GPa argon pressure, following an initial stress relief anneal at 982 $^{\circ}\text{C}$ for 0.5 h. Fig. 6 shows a similar 3-D microstructural architecture composite for a z -axis oriented cylinder built in

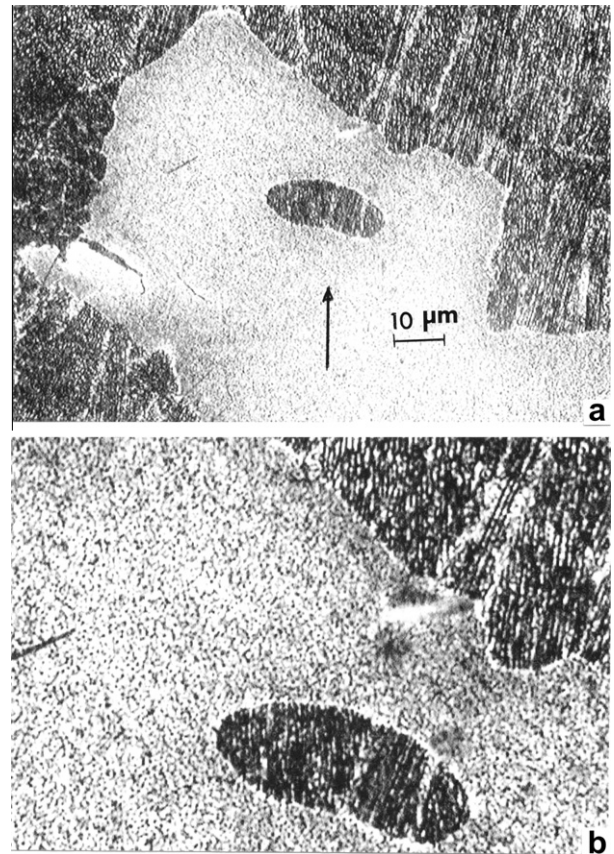


Fig. 7. (a) Vertical reference section (OM) views showing partial recrystallization for an x -axis fabricated cylinder in nitrogen and HIP in argon. The arrow shows the build direction. (b) A magnified view of (a).

argon gas and HIP as noted for Fig. 5. Fig. 7 shows a vertical section reference view for an SLM fabricated x -axis cylinder built in a nitrogen gas environment and HIP as

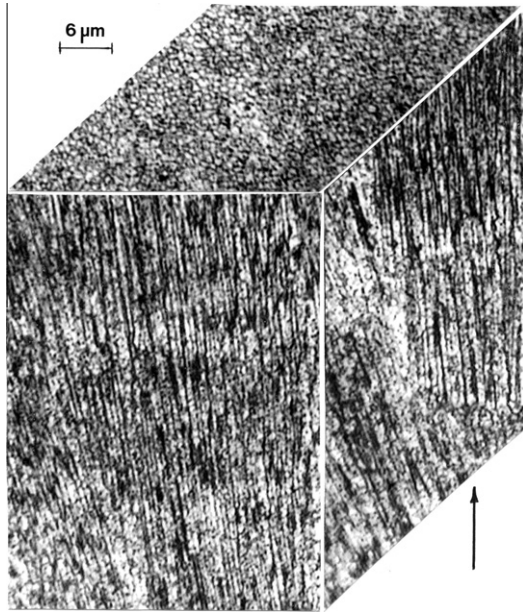


Fig. 8. 3-D OM composite view for a cylindrical component (x -axis) fabricated in nitrogen and HIP in argon. The build direction is indicated by the arrow (bottom right).

noted for Figs. 5 and 6. Fig. 7 shows some recrystallized areas exhibiting a relatively uniform dense distribution of precipitates, with remnants of the columnar microstructural architecture shown in Fig. 4 for the as-fabricated product and in Figs. 5 and 6 for as-fabricated and HIP products. Fig. 8 represents a 3-D composite for the as-fabricated (in nitrogen gas) and HIP x -axis cylindrical component, which is essentially identical to the 3-D composite columnar microstructural architectures shown in Figs. 5 and 6.

The columnar microstructural architectures shown in Figs. 4–8 are similar to those observed in alloy 625 components recently fabricated by electron beam melting (EBM) [8], where the columns were observed to be composed of γ'' -bct Ni_3Nb precipitates with spatial dimensions of $\sim 2 \mu\text{m}$, was more than twice that observed in Figs. 4–8. Strondl et al. [6] have also shown similar microstructural features in Inconel 718 fabricated by EBM, but the columnar γ'' architecture was not described in detail.

Fig. 9 compares the XRD analysis for the pre-alloyed Inconel 718 precursor powder with the horizontal and vertical reference plane spectra for a z -axis oriented cylinder in Ar. The powder XRD spectra (Fig. 9a) are coincident with solid solution γ -face-centered cubic (fcc) NiCr ($a = 0.359 \text{ nm}$, space group Fm-3m) and exhibit a prominent (1 1 1) texture. In comparison, the XRD spectra for the as-fabricated Inconel 718 components (in both Ar and N_2) exhibited mixed (1 1 1) and (200) texture peaks in the horizontal reference plane (Fig. 9b) and in the corresponding vertical reference plane (Fig. 9c) for both z -axis and x -axis oriented cylinders. The strong (200) texture is consistent with the EBM fabrication of Inconel 718 products by Strondl et al. [6], where γ -fcc grains were oriented with $\langle 100 \rangle$ parallel to the build direction and rep-

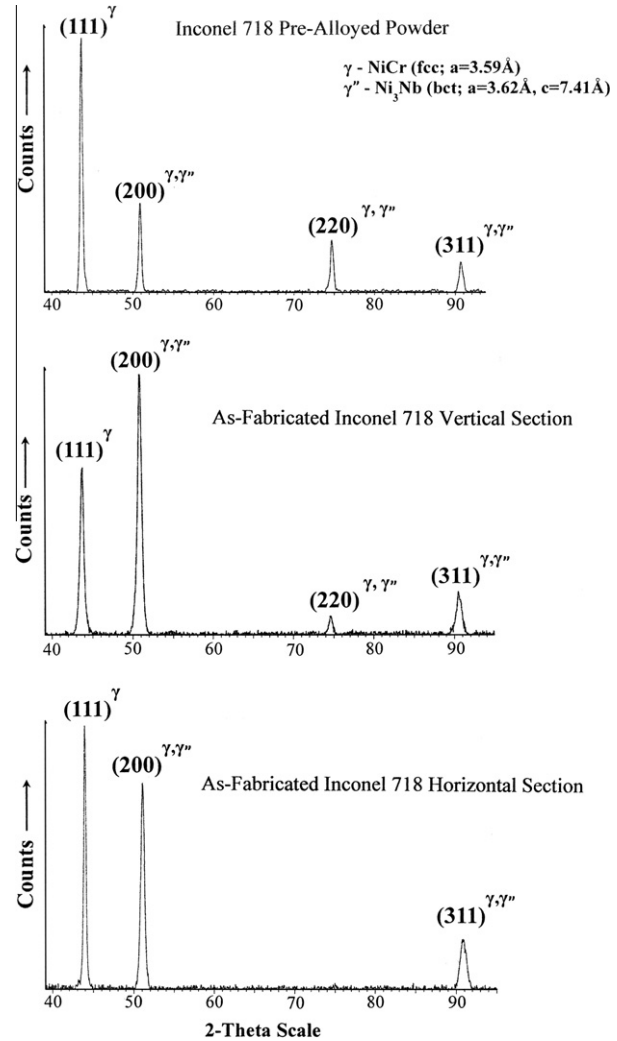


Fig. 9. XRD spectra for (a) precursor Inconel 718 powder and (b and c) as-fabricated (z -axis) cylinder prepared by EBM in argon for (b) the horizontal reference plane and (c) the vertical reference plane.

resented a “strong cube solidification and growth texture, almost like a single crystal”.

The γ'' -bct Ni_3Nb precipitate diffraction spectra coincide (or overlap) with the γ -fcc matrix spectra as shown in Fig. 9b and c for $200\gamma||200\gamma''$ as well as $220\gamma||200\gamma''$. However, this does not provide unambiguous evidence for γ'' -bct precipitation composing the columnar microstructural architectures in Figs. 5, 6 and 8, because γ -fcc ($a = 0.361 \text{ nm}$, space group Fm-3m) precipitate spectra can essentially coincide with all of the γ -fcc NiCr matrix spectra as well as the $\gamma''200$ and 220 spectral peaks. Consequently, unambiguous identification of γ' and γ'' precipitates must rely on TEM observations of particle morphologies and dimensions, and especially SAED patterns and corresponding, systematic dark field imaging, as illustrated in much earlier work on Inconel 718 ingots and related products by Paulonis et al. [9], Kirman and Warrington [3], Oblak et al. [10], Sundararaman et al. [5], and He et al. [11].

Fig. 10 shows a magnified 3-D TEM image composite corresponding to a section of Fig. 6 which illustrates a

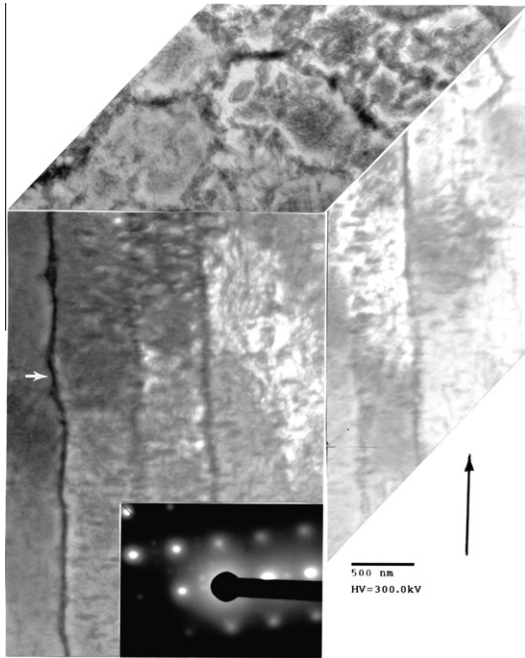


Fig. 10. 3-D TEM image composite view for an as-fabricated (in argon) z -axis cylinder HIP in argon. (Inset) The SAED pattern corresponds to a γ [001] zone in the vertical reference plane, as shown. The arrow to the right indicates the build direction.

variety of dense precipitates within these columnar [100] arrays and composing the apparent array boundaries. The horizontal surface view in Fig. 10 shows oblate ellipsoidal or spheroidal particles as large as 250 nm (major axis dimension) immersed in a dense field of precipitates <10 nm in diameter inside or in the boundaries of equiaxed arrays. Well-defined columnar arrays of elongated precipitates coincident with (100) are observed in the vertical reference plane in Fig. 10, parallel to the build direction (arrow). These crystallographic features are shown by the (010) SAED pattern insert in the forward vertical reference plane in Fig. 10. The columnar precipitate arrays are also parallel to columnar very low angle grain boundaries, indicated by the arrow to the left in the vertical reference plane in Fig. 10. From the 3-D TEM composite in Fig. 10 it is impossible to delineate between the cylindrical-like columnar precipitate arrays and the columnar grain boundaries or columnar grains, many of which have a [100] (200) texture, as shown in the corresponding XRD spectra in Fig. 11. Fig. 11 shows, in contrast to Fig. 9b and c, that the HIP/anneal process altered the texturing of the columnar precipitate arrays shown in Figs. 5, 6 and 8, producing a dominant (200) texture in the horizontal reference plane and (200) and (220) texture in the vertical reference plane. The (200) texture is reflected in the (001) SAED pattern insert in Fig. 10.

Fig. 12 shows the details of a vertical reference plane section of columnar precipitates stacked like dinner plates, and coincident with the fcc matrix (100) planes. The elongated precipitates appear to be oblate spheroids or

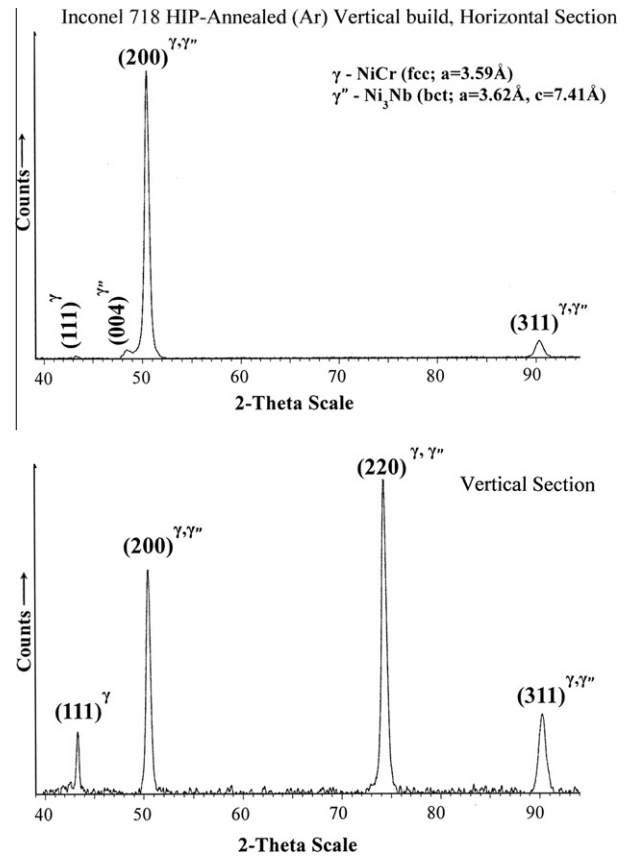


Fig. 11. XRD spectra of an as-fabricated and HIP (in argon) z -axis oriented specimen. (a) Horizontal reference plane (normal to the build direction). (b) Vertical reference plane (parallel to the build direction).

ellipsoids with the long axis (major axis dimension) coherent with the (100) planes of the fcc (NiCr) matrix. This is observed from the SAED (001) diffraction pattern insert which clearly shows the γ'' -bct diffraction spots and streaking of these spots in the [100] direction perpendicular to the major axis of the precipitates. Only the {100} (shown at (1) in Fig. 12) and $\{1/210\}$ and $\{1/20\}$ type (bct) superlattice reflections (shown at (2) in Fig. 12) for γ'' precipitates appear in the SAED pattern insert in Fig. 12. The columnar stacks of γ'' precipitates in Fig. 12 (parallel to the build direction shown by the arrow) are ~ 250 nm wide, with precipitate thicknesses of ~ 25 – 50 nm, spaced at the same distance. In Fig. 12 the propensity of γ'' precipitates are coincident (coherent) with the (100) planes while some are observed to be coincident with the other (010) variant. Dense and often irregular arrangements of various geometries and very small (regular) sizes of precipitates (γ'') also occur throughout the NiCr (fcc) matrix.

In retrospect, comparing and examining Figs. 3, 4–6, 8, 9 and 11, as well as Figs. 10 and 12, provides a conceptual mechanistic view of the SLM build process producing columnar (textured) grains and γ'' precipitate arrays. Fig. 13 provides a schematic composite showing these features as they relate to the scan geometry and melt pool related layer development, as well as the columnar arrays

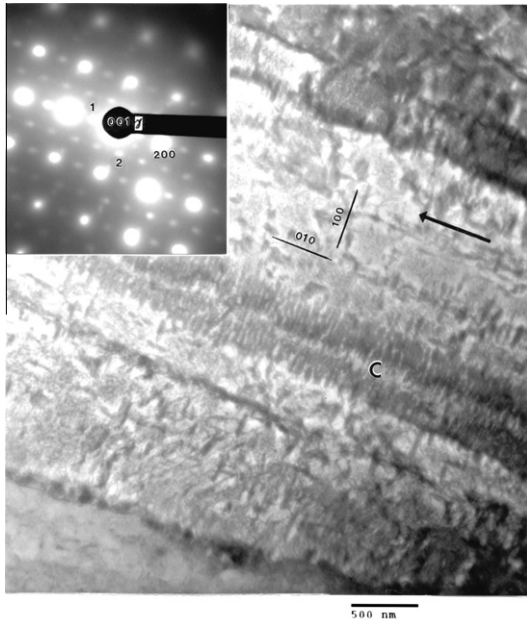


Fig. 12. Magnified TEM bright field image for a vertical reference plane section corresponding to Fig. 10. Lenticular-like/oblate ellipsoidal γ'' precipitates are coherent with $\{100\}$ planes in two prominent columns (c) which are parallel to the build direction noted by the large arrow. Some precipitates are coincident with the $\{010\}$ variant shown. (Inset) The SAED pattern shows a $\gamma[001]$ zone axis. $\gamma''\langle\bar{1}00\rangle$ and $\langle 1\frac{1}{2}0\rangle$ reflections are indicated by the spots designated 1 and 2, respectively.

formed as directional, epitaxial-like solidification phenomena related to the high temperature gradients occurring during the SLM process. The stacks of disc-like or oblate spheroidal γ'' precipitates implicit in Fig. 12 appear to be created in successively formed melt pools as a consequence of their short interaction times and high conductive heat transfer, possibly facilitated by the argon or nitrogen gas environments, or their corresponding thermal conductivities. In this regard, it is interesting to consider that while the thermal conductivities (K_T) of nitrogen and argon are 0.026 and 0.018 $\text{W m}^{-1} \text{K}^{-1}$ respectively at 300 K, they both increase linearly up to more than 2000 K [12]. Correspondingly, $K_T(\text{N}_2)/K_T(\text{Ar})$ 1.4. While we have not observed any notable microstructural variances between specimens fabricated by SLM in nitrogen versus argon gas (corresponding to Figs. 6 and 8, for example), there may be subtle differences in properties for components fabricated in these gases utilizing the same build or scan strategies (or parameters).

While the HIP/annealed specimens were only slightly recrystallized, as shown in Fig. 7, the recrystallized regions exhibited a dense, homogeneous precipitate distribution (Fig. 7b). However, recrystallization was considerably more extensive for the as-fabricated components annealed in Ar at standard pressure for 4 h at 1160 °C. This feature is illustrated in Figs. 14 and 15a, which show corresponding horizontal and vertical reference plane observations for an x -axis oriented cylinder fabricated in argon. Because of the etching only traces of recrystallized grain boundaries are observed in Fig. 14, while Fig. 15a shows remnants of the melt pool layering in the vertical plane parallel to the build direction noted by the arrow. By tailoring the etchant

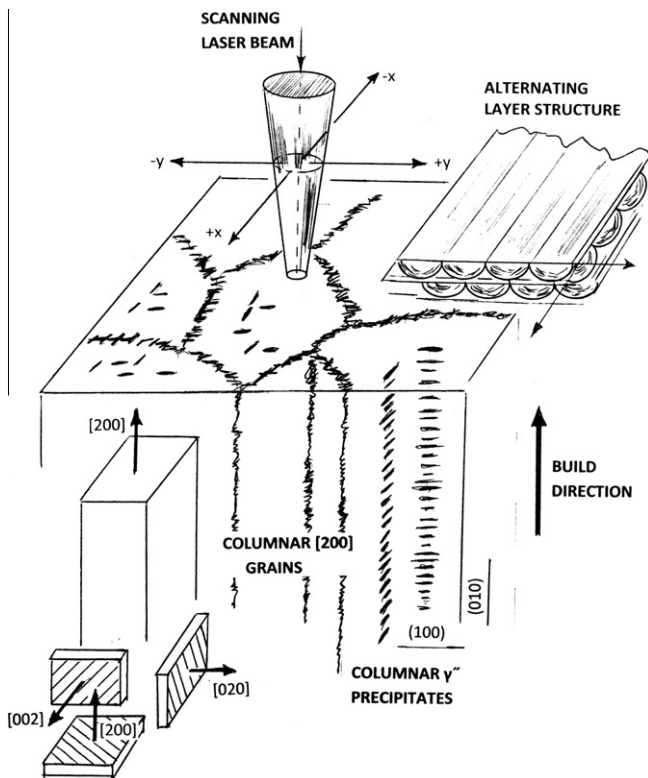


Fig. 13. Schematic views illustrating the directional solidification-induced columnar grains and γ'' precipitate arrays as well as the melt pool/layer structure development in SLM. The coincident plane variants for (100) $[200]$ are shown at $[002]$, $[200]$ and $[020]$.

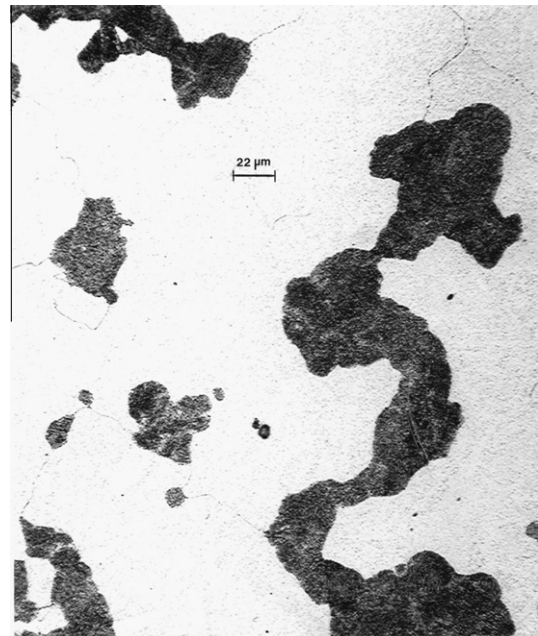


Fig. 14. Horizontal reference plane (OM) view for recrystallized microstructures following as-fabricated (argon) and annealed treatment (argon) for an x -axis oriented cylinder.

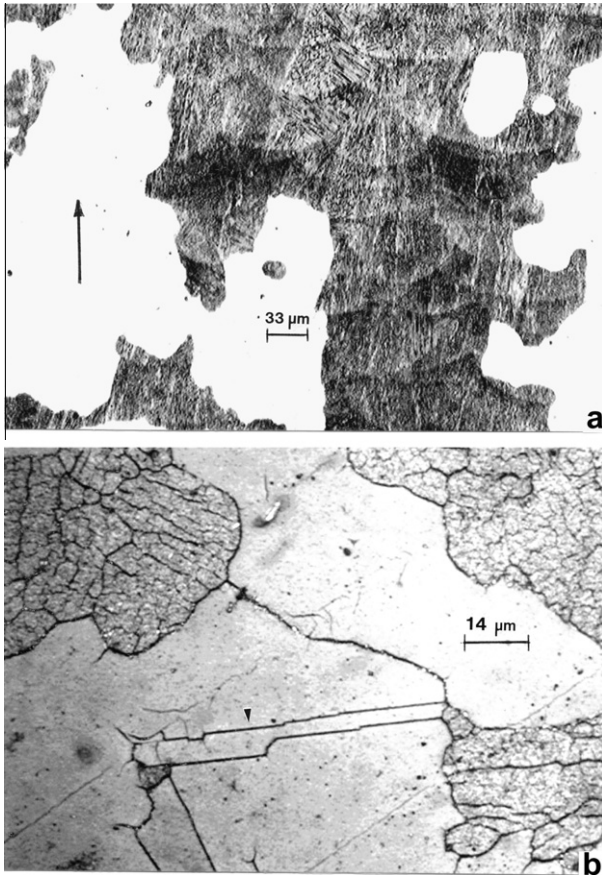


Fig. 15. (a) Vertical reference plane (OM) view for recrystallized microstructures corresponding to Fig. 3, showing melt pool interaction and layering in remnant columnar microstructure. The arrow denotes the build direction. (b) Horizontal plane reference (OM image) corresponding to (a) after etching to reveal the recrystallized grain and annealing twin (γ) boundaries (arrow).

(5% HCl, 95% water) and electro-etching at 4 V for 0.5–1 min, both the recrystallized (NiCr-fcc) matrix grain and coherent twin boundary structure could be observed, as shown in Fig. 15b.

Fig. 16 shows, for comparison with Figs. 4–6 and 8, a 3-D composite view typical for the as-fabricated and annealed cylindrical samples. Unrecrystallized columnar γ'' precipitate zones (C) can be observed, in contrast to the recrystallized and re-precipitated fcc matrix (R) where, in contrast to the coherent γ'' oblate spheroidal/ellipsoidal precipitates in the columnar arrays, the precipitates in the recrystallized matrix in Fig. 16 are more regular (cuboidal or spherical), with apparent diameters from Fig. 16 of ~ 300 nm. XRD spectra obtained for the horizontal and vertical reference planes corresponding to Fig. 16 were, as shown in Fig. 17, similar to those of the as-fabricated and HIP components shown in Figs. 9 and 11, respectively, except for the variations in texture as a consequence of the more extensive recrystallization apparent in Fig. 16. The XRD spectra corresponding to Fig. 16 and shown for the horizontal and vertical reference planes in Fig. 17 are similar to those for the HIP/annealed components illustrated

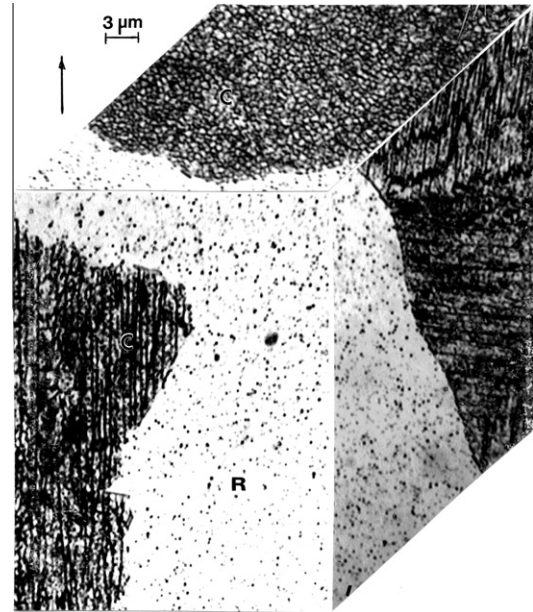


Fig. 16. 3-D OM composite view for the annealed (4 h at 1160 °C) argon fabricated x -axis cylinder. The recrystallized regions are denoted R. Selective etching reveals homogeneous globular precipitates. C indicates the original (remnant) columnar microstructural architecture arrays. The arrow at upper left denotes the build direction.

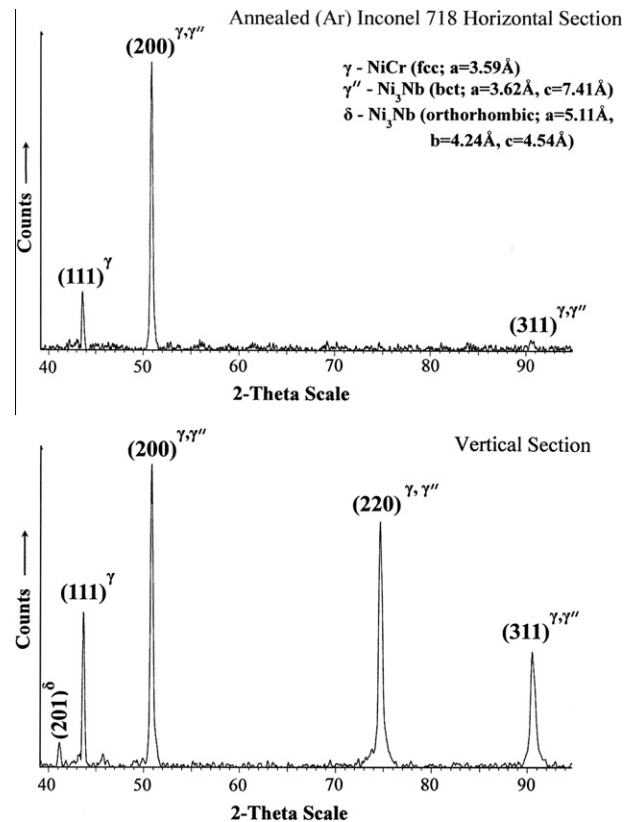


Fig. 17. XRD spectra representing the as-fabricated and annealed (4 h at 1160 °C) specimens corresponding to Fig. 16. (a) Horizontal reference plane. (b) Vertical reference plane.

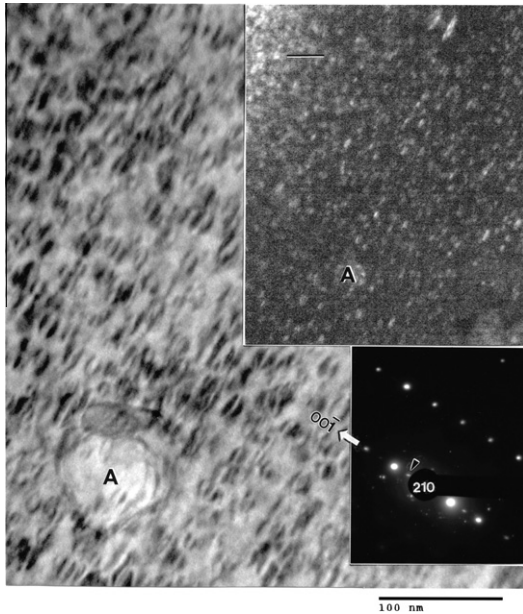


Fig. 18. TEM observation of dense γ'' precipitation in recrystallized regions for annealed SLM fabricated Inconel 718. The enlarged view shows oblate ellipsoidal γ'' precipitates coincident with (001) (or (0 0 $\bar{1}$)) planes while the low magnification dark field image insert shows these precipitates imaged with the [0 0 $\bar{1}$] (bct) reflection at the point indicated by the small arrow in the SAED pattern insert. The surface orientation is noted as the [210] fcc zone. A indicates a common reference for the enlarged view and the reduced magnification, dark field image insert. Note that the magnification bar in the dark field insert is the same as in the bright field image.

in Fig. 11. There is some additional prominence of (1 1 1) in both reference planes and some additional (200) and (220) prominence in the vertical reference plane for both Figs. 11 and 17. Both Figs. 11 and 17, representing annealing of the as-fabricated components, show some recognizable vari-

ances in spectral peak prominence, especially suppression of (1 1 1) and recognizable prominence of (220) in the vertical reference plane parallel to the build direction. Fig. 11a shows a (004) γ'' peak not present in other XRD spectra (Figs. 9 and 17), while Fig. 17b shows a new peak for the Ni_3Nb orthorhombic (δ) phase indexed as (201) δ ($a = 0.51$ nm, $b = 0.42$ nm, $c = 0.45$ nm, space group Pmmn). The δ phase is also referred to by some investigators as the β phase [13]. While the precipitates distributed within the recrystallized regions (marked R in Fig. 16) may be γ' -fcc Ni_3Nb , the corresponding spectral peaks overlap the fcc NiCr matrix peaks, since the lattice parameters only differ by 0.012 nm (0.3%). Correspondingly, except for the (004) γ'' spectral peak in Fig. 9a, there is no clear delineation of the precipitate identity in the XRD patterns (Figs. 9, 11 and 17), as noted previously.

Fig. 18 illustrates this feature for a typical recrystallized region in the horizontal reference plane characterized by Fig. 16. The magnified TEM image in Fig. 18 shows oblate ellipsoidal γ'' precipitates having an average minor axis dimension of ~ 7 nm and a major axis coincident with {001} of ~ 35 nm, or a ratio $D/d = 5$. The reduced magnification dark field image insert in Fig. 18 shows these aligned γ'' precipitates using the [0 0 $\bar{1}$] reflection indicated by the small arrow in the SAED pattern insert in Fig. 18. The white arrow in Fig. 18 illustrates the [0 0 $\bar{1}$] direction, which is perpendicular to the coincident (001) planes. This dense γ'' precipitate occurrence is similar to the observations of Slama et al. [13] for aging of Inconel 718 at 750 °C for 4–98 h and He et al. [11] for solution treatment of Inconel 718 up to 1050 °C for 1 h. The interesting feature of the present observations (in Fig. 18) is the dense arrangement of fine γ'' precipitates which have re-precipitated 100 °C above this temperature, although the 4 h anneal corresponded to the aging time for the optimum

Table 1

Mechanical properties of Inconel 718 cylindrical components fabricated by selective laser melting (SLM) in argon or nitrogen.

| Tensile orientation ^a and processing condition ^b | Argon | | | | | Nitrogen | | | | |
|--|--------------------------|------------------|--------------------------|------------------|-------------------|--------------------------|------------------|--------------------------|------------------|-------------------|
| | Hardness | | Tensile properties | | | Hardness | | Tensile properties | | |
| | HV ^d (GPa) | HRC ^d | Y ^e (0.2%) | UTS ^f | Elongation (%) | HV ^d (GPa) | HRC ^d | Y ^e (0.2%) | UTS ^f | Elongation (%) |
| <i>z</i> -Axis, as-fabricated | | | | | | | | | | |
| <i>x</i> -Axis, as-fabricated | 3.8/3.9 | 30/33 | | | | | | 0.83 | 1.12 | 25 |
| <i>z</i> -Axis, HIP + annealed | 5.6/5.8 | 38/39 | 0.85 | 1.14 | 28 | 5.5/5.6 | 35/38 | 0.88 | 1.14 | 30 |
| <i>x</i> -Axis, HIP + annealed | 5.5/5.8 | 33/35 | 0.89 | 1.2 | 28 | 5.4/5.6 | 36/38 | 0.93 | 1.2 | 27 |
| <i>x</i> -Axis, annealed (4 h) | 4.5/4.7 | 39/40 | | | | | | | | |
| Nominal ^c , wrought (annealed) | | 24 | 0.83 | 1.1 | 31 | | | | | |
| Nominal ^c , wrought (aged) | | 45 | 1.4 | 1.6 | 16 | | | | | |

^a Tensile orientation refers to the build convention shown in Fig. 3b. *z*-Axis refers to cylinders built parallel to the build direction; *x*-axis refers to cylinders built perpendicular to the build (or beam) direction.

^b Processing conditions: as-fabricated, fabricated cylinders stress relief annealed at 982 °C for 0.5 h under vacuum and HIP at 1163 °C for 4 h in argon at 0.1 GPa pressure; HIP + annealed, fabricated cylinders annealed in argon at 1160 °C for 4 h; annealed, annealed for 4 h.

^c Nominal wrought Inconel 718 data from Special Metals Corp. (www.specialmetals.com).

^d Vickers microindentation hardness (HV) and Rockwell C-scale hardness (HRC) are measured in the horizontal plane/vertical plane normal to or parallel to the build direction (Fig. 3b).

^e 0.2% Engineering offset yield strength in GPa. The data is the average of four tests.

^f UTS (ultimate tensile strength) in GPa. The data is the average of four tests.

volume fraction of precipitates. The γ'' precipitate dimensions shown in Fig. 18 are also consistent with those observed for Inconel 718 aging at 750 °C for 4 h [13] and up to 1050 °C for 1 h [11].

The occurrence of the δ phase (or β phase, orthorhombic Ni_3Nb) in the XRD spectrum in Fig. 17 was observed at grain boundaries or, more specifically, those boundaries characterizing the recrystallization front separating the unrecrystallized γ'' regions from the recrystallized regions illustrated typically in Fig. 16. This interfacial occurrence of δ precipitates is characteristic of many earlier observations in grain boundaries of annealed wrought Inconel 718 alloy [5,11,13–15].

3.2. Analysis and comparison of the mechanical behavior: hardness and tensile measurements

Wrought Inconel 718 has largely been used for critical components in turbine engine fabrication because of its relatively good mechanical properties up to about 700 °C. The γ'' phase is the principal strengthening agent [5,11,13–15], especially during isothermal aging in the temperature range 550–900 °C [13,15,16]. While the present study has not involved systematic aging, hardness and tensile strength measurements have been made and compared, as illustrated in Table 1.

Table 1 compares hardness (both Vickers (HV) and Rockwell C-scale (HRC)) measurements along with the tensile behavior of SLM fabricated cylinders, fabricated and HIP cylinders, and fabricated and annealed cylinders with selected orientations and in argon or nitrogen gas atmospheres. These selected measurements are also compared with nominal wrought and annealed Inconel 718 and aged 718 alloy mechanical behavior. It can be observed that the Vickers microindentation hardness for the SLM x -axis oriented cylinder components fabricated in argon averaged ~ 3.9 GPa for the horizontal and vertical reference planes, while the corresponding HIP component averaged 5.7 GPa, in contrast to 4.6 for the SLM fabricated and annealed (4 h at 1160 °C) component. These hardness results can be compared with the microindentation hardness evolution for isochronal tempering (for 4 h) of wrought Inconel 718 in the temperature range 500–850 °C determined by Slama et al. [13]. In this work [13] the hardness (HV) between 500 and 600 °C remained constant at 2.8 GPa, while samples quenched from 990 °C had a hardness of 2.5 GPa. After tempering at 650 °C the hardness was 3.5 GPa. The maximum hardness of 4.7 GPa occurred at 750 °C, decreasing to 4 GPa at 800 °C for 4 h and to 2.8 GPa at 850 °C. Corresponding HRC values for the SLM fabricated components as well as the HIP samples averaged 32 and 40 HRC, respectively, in contrast to wrought, annealed, and aged values of 24 and 45 HRC, respectively.

While the measured hardnesses in Table 1 for the SLM fabricated and treated cylinder components are comparable with the behavior of wrought Inconel 718, the yield (Y) and

ultimate tensile strength (UTS) slightly exceed the wrought/annealed products, while the elongation is essentially the same. However, the aged wrought Inconel 718 strength (yield and UTS) exceeds the SLM fabricated and treated products, although the elongation is significantly reduced. There is a consistent variance of yield and UTS for the x -axis oriented specimens and the z -axis oriented specimens (between 5% and 6%) for both the argon atmosphere fabricated cylinders and the nitrogen atmosphere fabricated components. This difference is due primarily to the variance in the directional columnar grains and γ'' microstructural architecture relative to the tensile axis. While there is a comparable variance in the 0.2% offset yield strength between the argon and nitrogen gas atmospheres, there is no corresponding UTS or elongation variance, and it is concluded that the gas environment (argon or nitrogen) did not significantly influence the corresponding SLM built components. There were also no corresponding microstructural (γ'') variances for specimens fabricated in argon or nitrogen and correspondingly treated.

4. Summary and conclusions

The SLM fabrication of cylindrical components of Inconel 718 from a pre-alloyed powder in both argon and nitrogen atmospheres produces an unusual columnar microstructural architecture composed of primarily $\langle 200 \rangle$ textured γ'' phase precipitate columns within directionally solidified and similarly textured grains. The γ'' -bct phase (Ni_3Nb) precipitates were coincident and coherent with the γ -fcc matrix $\{001\}$ and $\{010\}$ planes for $[200]$, and also $\{100\}$ for $[020]$ or $[002]$ texture. These findings are completely consistent with those for wrought Inconel 718 alloy characterized in detail over the past several decades.

In the as-fabricated form the γ'' phase precipitates are oblate spheroids/ellipsoids nominally measuring 100 nm in the major axis dimension (D) and 25 nm in the minor axis dimension (d) ($D/d = 4$). The corresponding microindentation hardness for specimens fabricated as horizontal cylinders with their axis perpendicular to the scan build direction (x -axis orientation) was 3.9 GPa. Upon hot isostatic pressing in argon at 1163 °C for 4 h (preceded by a stress relief anneal at 982 °C for 0.5 h) the Vickers microindentation hardness increased to 5.7 GPa for the same cylinder orientation. There was a marked preference for $\langle 200 \rangle$ texture and the γ'' phase precipitate columns become more regular, producing arrays spaced at ~ 0.8 μm . Hot isostatic pressing also resulted in a 5–10% volume fraction of recrystallized material in which the γ'' phase precipitate columns dissolved, and a homogeneous precipitation of primarily coherent spherical or cuboidal-like precipitates occurred. There was a 5–6% variance in the strength of cylinders fabricated in the x -axis orientation (normal to the build direction) or the z -axis orientation (parallel to the build direction) as a consequence of the orientation of the columnar γ'' phase architecture: parallel to the z -axis cylinder axis and perpendicular to the x -axis cylinder axis and,

correspondingly, parallel and perpendicular to the tensile axes, respectively.

SLM fabricated and annealed (1160 °C for 4 h) cylinders exhibited a much higher volume fraction of recrystallized γ -fcc material (>50%) and were characterized by the same homogeneous distribution of spherical γ' precipitates along with a few volume percent of δ phase (orthorhombic) Ni_3Nb nucleated at the unrecrystallized/recrystallized grain boundaries (interfaces). There was a small (~ 25 nm) wide denuded zone separating these δ phase precipitates from a high density of coherent γ'' phase precipitates composing the background of the recrystallized areas, in which the homogeneous cuboidal/spherical γ' precipitates occurred. These fine γ'' precipitates averaged 35 nm along their major axis and ~ 7 nm along the minor (oblate) axis ($D/d = 5$), in contrast to the larger precipitate sizes in the as-fabricated and as-fabricated and HIP components noted above. The corresponding microindentation hardness (HV) was 4.6 GPa, about 24% lower than the HIP samples but still 18% higher than the as-fabricated samples. There was no apparent or consistent variance in mechanical behavior of Inconel 718 alloy components fabricated in argon or in nitrogen.

Acknowledgements

We are grateful to LPW Technology Ltd., Maumee, OH, for providing the pre-alloyed Inconel 718 powder.

Portions of this research were also supported by a Mr. and Mrs. MacIntosh Murchison Endowed Chair at the University of Texas at El Paso.

References

- [1] Mehrabian R, Kear BH, Cohen M, editors. Rapid solidification processing. Baton Rouge, LA: Claitor's Publishing Division; 1978.
- [2] Patterson RJ, Cox AR, vanReuth EC. J Metals 1980;32(9):34–9.
- [3] Kirman I, Warrington OH. J Inst Metals 1971;99:197–202.
- [4] Cozar R, Pineau A. Metall Trans 1973;4:47–59.
- [5] Sundararaman M, Mukhopadhyay P, Banerjee S. Metall Trans 1992;23A:2015–28.
- [6] Strondl A, Fischer R, Frommeyer G, Schneider A. Mater Sci Eng A 2008;480A:138–47.
- [7] Thijs L, Verhaeghe F, Craeghs T, VanHumbeeck J, Kruth J-P. Acta Mater 2010;58:3303–12.
- [8] Murr LE, Martinez E, Gaytan SM, Ramirez DA, Machado BI, Shindo PW, et al. Metall Mater Trans A 2011;42A:3491–508.
- [9] Paulonis DF, Oblak JM, Duvall DS. Trans ASM 1969;62:611–6.
- [10] Oblak JM, Paulonis DF, Duvall DS. Metall Trans 1974;5:143–51.
- [11] He J, Fukuyama S, Yokogawa K. J Mater Sci Technol 1994;10:293–303.
- [12] Faubert FM, Springer GS. J Chem Phys 1972;57:2333–40.
- [13] Slama C, Serrant C, Cizeron G. J Mater Res 1997;12(9):2298–316.
- [14] Azadian S, Liu-Ying W, Warren R. Mater Charact 2004;53:7–16.
- [15] Li RB, Yao M, Liu WC, He XC. Scripta Mater 2002;46:635–8.
- [16] Eiselstein HL. Advances in the technology of stainless steels and related alloys, ASTM STP 369. West Conshohocken, PA: ASTM International; 1965. p. 62–70.